Quantum optimal control of unbounded molecular dynamics: Application to NaI predissociation

doi: 10.1063/1.1504701

Quantum optimal control of unbounded molecular dynamics: Application to NaI predissociation

Kazuyuki Nakagami, Yukiyoshi Ohtsuki,[a] and Yuichi Fujimura
Department of Chemistry, Graduate School of Science, Tohoku University, Sendai 980-8578, Japan

(Received 29 October 2001; accepted 15 July 2002)

In order to achieve optimal control of unbounded molecular dynamics, we develop an algorithm to deal with a spatially delocalized final condition of homogeneous pulse design equations that are derived from a typical optimal control procedure. We introduce a quasiprojector to specify a spatially delocalized physical objective, while we store wave packet components that spread beyond the grid region in memory. The quasiprojector, which can explicitly identify target products in photodissociation and bimolecular reactions, is a weighted sum of projectors, whose weight function is constant outside the grid region. This algorithm, combined with an efficient iteration method, is applied to the control of NaI predissociation with the aim of obtaining a high dissociation probability within one cycle of nuclear vibration. We discuss how the control mechanisms are changed depending on the potential coupling strengths and restriction imposed on the optical interaction region. The effects of molecular orientation on a control pathway are also examined using a two-orientation model with the assumption of a frozen rotational wave packet. © *2002 American Institute of Physics.* [DOI: 10.1063/1.1504701]

I. INTRODUCTION

Laser pulse design algorithms based on optimal control theory are presented in the form of inverse problems.[1–3] A standard variational procedure will give coupled nonlinear pulse design equations that satisfy both an initial condition and a final condition specified by a physical objective. Typically, optimal pulses are designed to achieve the largest transition probability from an initial state to an objective state while minimizing the pulse fluence. In this case, the pulse design equations have a homogeneous form, and the numerical implementations of the equations have been considerably improved by recently developed rapid convergent iteration algorithms.[4–7] Within the wave function formalism, the final condition is expressed as a wave function at a final time multiplied by a target operator that specifies a physical objective.[4,5]

Even if we restrict ourselves to this class of pulse design equations, there still remain numerical difficulties when dealing with unbounded molecular dynamics, since we have to use a spatially finite grid. When a wave packet spreads over a very large spatial region beyond a grid region, further propagation would cause fictitious reflection from the grid's edge. Another problem originates from a physical objective if specified by a spatially delocalized target operator, since it cannot be fully represented by a spatially finite grid. In this paper, we propose a numerical scheme that overcomes these difficulties and enables us to calculate optimal pulses that control unbounded dynamics.

For delocalization of a wave packet, introduction of the interaction representation[8] can, at least in principle, provide a way to prevent the wave packet from propagating outside the grid region. In our model calculations, however, we could not achieve the numerical accuracies required for our present purpose. The most frequently adopted methods are an optical-potential method (an absorbing boundary approach (Refs. 9–11) and its variants such as a wave packet splitting procedure.[12] In the latter,[12] the wave packet is divided into two components belonging to regions $\mathbf{R}$ and $1-\mathbf{R}$ using a cutoff function $f(q)$. Here the region $\mathbf{R}$ must be within the grid region, while $1-\mathbf{R}$ includes the region outside the grid, i.e., the asymptotic region. The cutout components of the wave packet can be stored in memory.[13]

A serious problem arises when a spatially delocalized physical objective is specified by a spatially delocalized target operator. This is because the final condition is given by the result of the target operator acting on a wave packet at a final time. That is, to determine a final condition of pulse design equations, an expression for the asymptotic components of the wave packet is required. When these asymptotic components are not available because of a small grid region, it is generally impossible to calculate backward time propagation that is involved in the pulse design equations. To overcome the difficulties originating from the spatially delocalized nature of the unbound dynamics, we propose a novel numerical algorithm in which a quasiprojector, which is defined in Sec. II, is introduced to specify a spatially delocalized objective. This algorithm makes it possible to calculate the backward propagation using the wave packet data stored in memory under certain conditions. As shown in Sec. II, these conditions do not severely limit its practical applicability. Since our numerical implementation for treating a final condition can be naturally combined with recently developed rapid convergent iteration solutions,[4–7] it offers a useful tool for calculating optimal pulses for unbounded molecular dynamics.

The quasiprojector can explicitly specify an objective

[a]Electronic mail: ohtsuki@mcl.chem.tohoku.ac.jp

state in an asymptotic region on a specified electronic state. It is thus useful for identifying particular photodissociation components, bimolecular reaction products, and so on. The question arises here as to whether there is a conventional alternative for treating the same class of problems without introducing a spatially delocalized target operator. For example, it is possible to measure a target product by accumulating the probability flux of it near the end of grid.[14] This, however, introduces an inhomogeneous term into the pulse design equations, which is not to easy to deal with numerically.

Due to the above-mentioned numerical difficulties, there have been only a few reports on the optimal control of systems including unbound states. Gross *et al.*[14] calculated optimal pulses that control the selectivity of dissociation channels in curve-crossing systems, but they used inhomogeneous pulse design equations. On the other hand, Somlói *et al.*[15] and de Vivie-Riedle *et al.*[16] used homogeneous design equations. The physical objective of Somlói *et al.*[15] was to efficiently cause the dissociation of I_2. In their study, since the wave packet always stayed within the grid region, there was no problem concerning the final condition. In the study by de Vivie-Riedle *et al.*,[16] laser-induced energy transfer reactions of Na-H_2 were investigated in terms of the wave packet localization. Their physical objective was the creation of a localized wave packet, and they did not examine artificial reflection of a wave packet. To the best of our knowledge, there is no report in which a solution algorithm for homogeneous pulse design equations with a spatially delocalized target in unbounded dynamics has been proposed.

This paper is organized as follows. After introducing pulse design equations (Sec. II A) and the wave packet splitting procedure (Sec. II B), we describe a solution algorithm for the backward time propagation in both the cases of a spatially localized and a delocalized target operator in Sec. II C. In Sec. III, the algorithm is applied to the control of NaI predissociation (a ''half-collision'' problem), in which we aim at accelerating the predissociation. In polyatomic molecules, predissociation often competes with various relaxation processes such as IVR (intramolecular vibrational-energy redistribution). It is thus important to analyze the optimal pathway to accelerate the predissociation using a simple molecule like NaI.[17,18] Finally, a summary and conclusions are given in Sec. IV.

II. THEORY

A. Optimal control pulse

We consider a molecule interacting with a time-dependent electric field, $E(t)$, through the semiclassical dipole-field interaction. The Hamiltonian of the system is given by

$$H^t = H_M + V^t = H_M - \mu E(t), \tag{1}$$

where H_M, V^t, and μ are the molecular Hamiltonian, interaction potential, and electric dipole moment operator, respectively. The electric field is assumed to be linearly polarized. The molecular Hamiltonian includes two kinds of coordinates, q and x, which represent continuum and bound states, respectively. It is expressed as

$$H_M = h(q) + h(x) + V(q,x) = H_0 + V. \tag{2}$$

In this paper, the time evolution of the system is assumed to be described by the Schrödinger equation

$$i\hbar \frac{\partial}{\partial t} |\psi(t)\rangle = H^t |\psi(t)\rangle, \tag{3}$$

with an initial condition of

$$|\psi(t=0)\rangle = |\psi_0\rangle. \tag{4}$$

The optimal pulse concerned here is designed so that it transfers as much of a population as possible into an objective state at a specified final time t_f subject to minimal pulse fluence. The objective state is specified by a target operator that has the largest expectation value when the molecular system reaches the objective state. Then we have the following objective functional to be maximized:

$$J = \langle \psi(t_f)|W|\psi(t_f)\rangle - \frac{1}{\hbar A}\int_0^{t_f} dt[E(t)]^2 - 2\,\mathrm{Re}\left\{ \int_0^{t_f} dt \langle \xi(t)| \left(\frac{\partial}{\partial t} + \frac{i}{\hbar} H^t \right) |\psi(t)\rangle \right\}, \tag{5}$$

where A, a positive constant, is chosen so as to weigh the significance of the penalty due to the pulse fluence and $|\xi(t)\rangle$ is a Lagrange multiplier constraining the system to obey the Schrödinger equation (3). As derived by means of the calculus of variations, the time evolution of the Lagrange multiplier is governed by the homogeneous equation of motion

$$i\hbar \frac{\partial}{\partial t} |\xi(t)\rangle = H^t |\xi(t)\rangle, \tag{6}$$

with a final condition of

$$|\xi(t_f)\rangle = W|\psi(t_f)\rangle. \tag{7}$$

To calculate optimal control pulses, it is evident that iteration methods need to be employed. For example, gradient methods[3,14,19–22] require the gradient $\delta J/\delta E(t)$ for $\forall t \in [0,t_f]$, which is given by

$$\frac{\delta J}{\delta E(t)} = -\frac{2}{\hbar}\,\mathrm{Im}\langle \xi(t)|\mu|\psi(t)\rangle - \frac{2}{\hbar A}E(t). \tag{8}$$

In other iteration algorithms,[4–7,23] on the other hand, the expression of the optimal pulse is explicitly used in the calculation:

$$E(t) = -A\,\mathrm{Im}\langle \xi(t)|\mu|\psi(t)\rangle. \tag{9}$$

Independent of an iteration algorithm, the coupled design equations of motion for $|\psi(t)\rangle$ and $|\xi(t)\rangle$ must be solved simultaneously. That is, in each iteration step, the Schrödinger equation is numerically integrated, starting with the initial condition. Using the wave function at the final time, the final condition of the Lagrange multiplier is calculated by Eq. (7), and then it propagates backward in time. The latter process originates from the fact that the optimal pulse design requires the solution of an inverse problem.

B. Splitting a wave packet

Let us introduce a cutoff function $f(q)$ to divide the wave packet into two components belonging to regions **R** and $1-\mathbf{R}$, where region **R** must be within the grid region.[12] Note that the function $f(q)$ is not a projector or a Hermitian operator. Here an electronic state is not explicitly specified for simplicity. If we need to explicitly specify an electronic state $|D(q)\rangle$, the cutoff function should be replaced with $f^{(D)}$ defined by

$$f^{(D)}=\int dq|Dq\rangle f(q)\langle Dq|, \tag{10}$$

where $|Dq\rangle=|D(q)\rangle|q\rangle$.

When the time interval is divided into N steps so that the nth time step corresponds to $t_n=n\Delta t$ with $\Delta t=t_f/N$ ($n=0,1,2,...,N$; $t_0=0$ and $t_N=t_f$), the calculation algorithm is summarized as follows.

(1) Splitting the initial wave packet:

$$\begin{aligned}|\psi(t_0)\rangle&=f|\psi(t_0)\rangle+(1-f)|\psi(t_0)\rangle\\&=|\phi_{\mathbf{R}}(t_0)\rangle+|\phi_{1-\mathbf{R}}(t_0)\rangle,\end{aligned} \tag{11}$$

where $|\phi_{1-\mathbf{R}}(t_0)\rangle$ is stored in memory.

(2) Calculating the time evolution within region **R**:

$$|\phi(t_n)\rangle=U(t_n,t_{n-1})|\phi_{\mathbf{R}}(t_{n-1})\rangle \quad (n=1,2,...,N), \tag{12}$$

where $U(t_n,t_{n-1})$ is a time evolution operator.

(3) Splitting the wave packet $|\phi(t_n)\rangle$:

$$\begin{aligned}|\phi(t_n)\rangle&=f|\phi(t_n)\rangle+(1-f)|\phi(t_n)\rangle\\&=|\phi_{\mathbf{R}}(t_n)\rangle+|\phi_{1-\mathbf{R}}(t_n)\rangle,\end{aligned} \tag{13}$$

where $|\phi_{\mathbf{R}}(t_n)\rangle$ is used in the next time step, (2), while $|\phi_{1-\mathbf{R}}(t_n)\rangle$ is stored in memory.

Once the cutout components of the wave packet $\{|\phi_{1-\mathbf{R}}(t_n)\rangle, n=0,2,...,N\}$, are stored in memory, we do not calculate their time evolution.[13] Since we have no information on the future behavior of the stored components, we cannot resume the calculation of their time evolution even if they return to region **R**. This algorithm is, thus, valid only when the cutout packet $\{|\phi_{1-\mathbf{R}}(t_n)\rangle\}$ never comes back into region **R** in a given time interval $[0,t_f]$. In other words, this algorithm can be applied even to bound systems as long as the cutout packets remain in region $1-\mathbf{R}$ during the control time. Using the notation introduced above, the wave function at time t_n can be formally expressed as

$$\begin{aligned}|\psi(t_n)\rangle&=|\phi_{\mathbf{R}}(t_n)\rangle+\sum_{m=0}^{n}U(t_n,t_m)|\phi_{1-\mathbf{R}}(t_m)\rangle\\&=|\phi_{\mathbf{R}}(t_n)\rangle+|\Phi_{1-\mathbf{R}}(t_n)\rangle.\end{aligned} \tag{14}$$

It should be noted again that the time evolution is calculated within region **R** and that we have no information on $|\Phi_{1-\mathbf{R}}(t_n)\rangle$.

C. Solution to the Lagrange multiplier with a spatially delocalized target operator

It is convenient to introduce projectors that specify the cutoff regions. Letting q_{R1} and q_{R2} be

$$q_{R1}=\min\{q:f(q)=1\} \tag{15a}$$

and

$$q_{R2}=\max\{q:f(q)=1\}, \tag{15b}$$

the projectors P and Q are defined by

$$P=\int_{q_{R1}}^{q_{R2}}|q\rangle dq\langle q| \tag{16a}$$

and

$$Q=1-P. \tag{16b}$$

According to these definitions, we have the relations

$$Pf=fP=P, \tag{17a}$$

$$P(1-f)=(1-f)P=0, \tag{17b}$$

and

$$1-f=Q(1-f)=(1-f)Q. \tag{17c}$$

Although the projectors do not appear in numerical calculations, the introduction of them makes it easy to develop solution algorithms because of their self-adjoint, idempotent, and orthonomal properties.

We first summarize the following preconditions that are required in our solution algorithm:

$$[\mathrm{P1}] \quad |\Phi_{1-\mathbf{R}}(t)\rangle=Q|\Phi_{1-\mathbf{R}}(t)\rangle \quad \text{for } \forall t\in[0,t_f]. \tag{18}$$

This condition means that the cutout packets $\{|\phi_{1-\mathbf{R}}(t_n)\rangle\}$ do not come back into region **R** in a given time interval $[0,t_f]$, which is the same assumption as that required in the wave packet splitting procedure described in Sec. II B.

$$[\mathrm{P2}] \quad QV^t=V^tQ=0. \tag{19}$$

We assume that the molecule-laser interaction occurs within the P space. *The preconditions [P1] and [P2] are assumed throughout this paper*.

$$[\mathrm{P3}] \quad QV=VQ=0. \tag{20}$$

This condition requires that the two kinds of degrees of freedom, represented by q and x, interact with each other only within the P space.

It should be noted that only a projected wave packet $P|\psi(t_n)\rangle$, rather than a whole packet, is needed to calculate optimal pulses because of condition [P2]. According to the algorithm described in Sec. II B, $P|\psi(t_n)\rangle$ is expressed as

$$P|\psi(t_n)\rangle=P|\phi_{\mathbf{R}}(t_n)\rangle, \tag{21}$$

where we have used Eqs. (14), (17c), and (18).

The final condition of the Lagrange multiplier is given, from Eqs. (7) and (14), by

$$|\xi(t_N)\rangle=W|\psi(t_N)\rangle=W[|\phi_{\mathbf{R}}(t_N)\rangle+|\Phi_{1-\mathbf{R}}(t_N)\rangle]. \tag{22}$$

Since the expression of $|\Phi_{1-\mathbf{R}}(t_N)\rangle$ is not available, it is generally impossible to determine the final condition $|\xi(t_N)\rangle$. As will be shown below, however, if the target operator W possesses appropriate properties, we can calculate $\{P|\xi(t_n)\rangle\}$ and thus obtain the optimal pulse.

1. Localized target operator

Before dealing with a spatially ''delocalized'' target operator, we briefly consider a localized target operator that satisfies the condition of

$$W = WP. \tag{23}$$

We call it a localized target operator. Since this target operator exclusively operates on the projected wave packet in region **R**, the final condition of the Lagrange multiplier can be written as

$$|\xi(t_N)\rangle = W|\psi(t_N)\rangle = WP|\psi(t_N)\rangle = W|\phi_{\mathbf{R}}(t_N)\rangle. \tag{24}$$

Once the final condition has been determined, the time evolution is calculated simply by integrating the equation of motion. If a portion of the Lagrange multiplier spreads beyond the grid region, we may add an optical potential to eliminate those components. If necessary, we can apply the cutoff function to the Lagrange multiplier and store cutout components in computer memory. In the latter case, the calculation algorithm is the same as that of the wave function propagation described in Sec. II B.

2. Delocalized target operator

Next, we consider a ''delocalized'' target operator that operates on the wave packet components in both regions **R** and $1-\mathbf{R}$. As proved below, if the target operator satisfies the condition of

$$W(x,q)Q = QW(x,q) = QW_B(x), \tag{25}$$

then $P|\xi(t_n)\rangle$ can be calculated under the preconditions of [P1–P3]. Here the operator $W_B(x)$ does not contain the q degrees of freedom. Examples of this kind of delocalized operator include one that specifies objective states concerned solely with the x degrees of freedom and a quasiprojector that specifies dissociation components, bimolecular reaction products, and so on. We will show one of the examples of the quasiprojector in Sec. III.

Suppose that the wave function and Lagrange multiplier evolve in time under electric fields $E^{(k)}(t)$ and $E^{(\ell)}(t)$, respectively, where the superscripts in the electric fields each denote the number of iteration steps. It should be noted that superscript (k) is not equal to (ℓ) in general because of the iterative nature of the solution. Using this notation, we shall express the wave function at a final time $t_f = t_N$ as

$$\begin{aligned}|\psi(t_N)\rangle &= |\phi_R(t_N)\rangle + \sum_{n=0}^{N} U^{(k)}(t_N,t_n)|\phi_{1-R}(t_n)\rangle \\ &= |\phi_R(t_N)\rangle + |\Phi_{1-R}^{(k)}(t_N)\rangle,\end{aligned} \tag{26}$$

where the superscript (k) in the time evolution operator corresponds to the electric field $E^{(k)}(t)$. In the following, we will use a simplified notation in which the time evolution operator during the time interval $[t_n, t_{n-1}]$ is represented by

$$U_n^{(k)} = U^{(k)}(t_n, t_{n-1}) = U^{(k)}(t_n, t_n - \Delta t). \tag{27}$$

At time t_N, the projected Lagrange multiplier $P|\xi(t_N)\rangle$ is given by

$$\begin{aligned}P|\xi(t_N)\rangle &= PW|\psi(t_N)\rangle = PW[|\phi_R(t_N)\rangle + |\Phi_{1-R}^{(k)}(t_N)\rangle] \\ &= PW|\phi_R(t_N)\rangle,\end{aligned} \tag{28}$$

where Eqs. (17c) and (25) have been used to derive Eq. (28).

At time t_{N-1}, the projected Lagrange multiplier $P|\xi(t_{N-1})\rangle$ is given by

$$\begin{aligned}P|\xi(t_{N-1})\rangle &= PU_N^{(\ell)\dagger}|\xi(t_N)\rangle \\ &= PU_N^{(\ell)\dagger}W|\psi(t_N)\rangle \\ &= PU_N^{(\ell)\dagger}W[|\phi_R(t_N)\rangle + |\phi_{1-R}(t_N)\rangle],\end{aligned} \tag{29}$$

where the relation proved in the Appendix,

$$PU_N^{(\ell)\dagger}WU_N^{(k)}|\Phi_{1-R}^{(k)}(t_{N-1})\rangle = 0, \tag{30}$$

has been used. Since this relation can be generalized to

$$PU_{n+1}^{(\ell)\dagger}U_{n+2}^{(\ell)\dagger}\cdots U_N^{(\ell)\dagger}WU_N^{(k)}\cdots U_{n+2}^{(k)}U_{n+1}^{(k)}|\Phi_{1-R}^{(k)}(t_n)\rangle = 0 \tag{31}$$

(Appendix), we can calculate $P|\xi(t_n)\rangle$ using stored wave packet data.

Therefore, if we introduce $|\xi_R(t_n)\rangle$, which connects with $P|\xi(t_n)\rangle$ through the relation

$$P|\xi(t_n)\rangle = P|\xi_R(t_n)\rangle, \tag{32}$$

our algorithm for calculating $|\xi_R(t_n)\rangle$ can be summarized as follows:

(1) final condition

$$|\xi_R(t_N)\rangle = W|\phi_R(t_N)\rangle, \tag{33}$$

(2) backward time propagation

$$|\xi_R(t_n)\rangle = U^{\dagger}(t_{n+1},t_n)[|\xi_R(t_{n+1})\rangle + W|\phi_{1-R}(t_{n+1})\rangle]. \tag{34}$$

Repeating Eq. (34) successively, $n = N-1 \to N-2 \to \cdots \to 1 \to 0$, we have $|\xi_R(t_n)\rangle$ and thus $P|\xi(t_n)\rangle$ [Eq. (32)], which are needed to calculate optimal pulses.

III. RESULTS AND DISCUSSION

Sodium iodide is a target molecule widely used for demonstrating quantum control. Experimentally, Herek *et al.*[24] controlled the branching ratio between two channels of photodissociation products (Na+I and Na*+I) based on a pump–dump scheme. Bardeen *et al.*[25] tried to improve the selectivity by squeezing the spatial distribution of the excited packet using chirped pulses. We theoretically designed control pulses that accelerate the predissociation of NaI using a local control method.[17,18] In this treatment, the reaction pathway and an objective state are predetermined by a target operator as an input.[2,17,18,26,27] On the other hand, the optimal control procedure naturally chooses optimal pathways to achieve a high probability of transition to the objective state subject to the minimum pulse fluence. As an application of the algorithm described in Sec. II, we will present numerical results on the optimal control of photodissociation of NaI, which is an example of a half-collision.

For illustrative purposes, we start with a one-dimensional, two-electronic state model adopted from Ref. 28 to describe the dynamics. The orientation effects on the control will be examined in Sec. III C. The dynamics of the

wave packet evolving on the first excited electronic state of NaI is determined by the interaction between the two diabatic states arising from ionic and covalent electronic configurations. In the diabatic representation, the molecular Hamiltonian is expressed as

$$H_M = H_0(q) = \sum_{D=i,c} \int dq|Dq\rangle[T + V_{DD}(q)]\langle Dq| + \left\{ \int dq|iq\rangle V_{ic}(q)\langle cq| + \text{H.c.} \right\}, \tag{35}$$

where $|iq\rangle = |i(q)\rangle|q\rangle$ ($|cq\rangle = |c(q)\rangle|q\rangle$) denotes the ionic (covalent) state with the eigenstate of the nuclear coordinate, $|q\rangle$. The operators T, $V_{ii}(q)$ [$V_{cc}(q)$], and $V_{ic}(q)$ [$V_{ci}(q)$] represent a kinetic energy operator, the diabatic potential of the ionic (covalent) state, and the coupling between the two diabatic states, respectively. For the electric dipole moment operator, we assume that it optically connects two diabatic states, and we neglect the nuclear coordinate dependence.[29] Some features of this model potential are described in our previous paper.[17]

In the simulations shown below, the final time is set to $t_f = 1000$ fs, which is shorter than the period of the wave packet oscillation in the electronic excited state. This time interval is divided into $N_t = 50\,000$ time steps. The convergence with respect to the number of time steps was checked numerically. For the internuclear distance, we assume a grid region of [1.5 Å, 15.0 Å], in which the $N_q = 512$ grid points are uniformly spaced. The time evolution is then calculated by the first-order split operator scheme together with the fast Fourier transform (FFT) method. The electronic transitions due to the optical as well as potential couplings are calculated using the Pauli matrix.[14,17] The cutoff function used to specify the out-of-region components of the wave function is set to

$$f^{(c)}(q) = \int dq|cq\rangle f(q)\langle cq|, \tag{36a}$$

where

$$f(q) = \frac{1}{1 + \exp[-\alpha_m(q - q_m)]}, \tag{36b}$$

with $\alpha_m = 10.0\ \text{Å}^{-1}$ and $q_m = 14.0$ Å. We checked that a reasonable choice of these parameters—for example, $(\alpha_m, q_m) = (4.0\ \text{Å}^{-1}, 15.5\ \text{Å})$—does not change the numerical results. Since our physical objective here is to accelerate the dissociation on the covalent potential, the target operator can be chosen as

$$W = \int_0^\infty dq|cq\rangle w(q)\langle cq|, \tag{37a}$$

where

$$w(q) = \frac{1}{1 + \exp[-\alpha_W(q - q_W)]}, \tag{37b}$$

with $\alpha_W = 4.0\ \text{Å}^{-1}$ and $q_W = 11.0$ Å. The functions of $f(q)$ and $w(q)$ are illustrated in Fig. 1 with the potential energy curves used in our calculations.

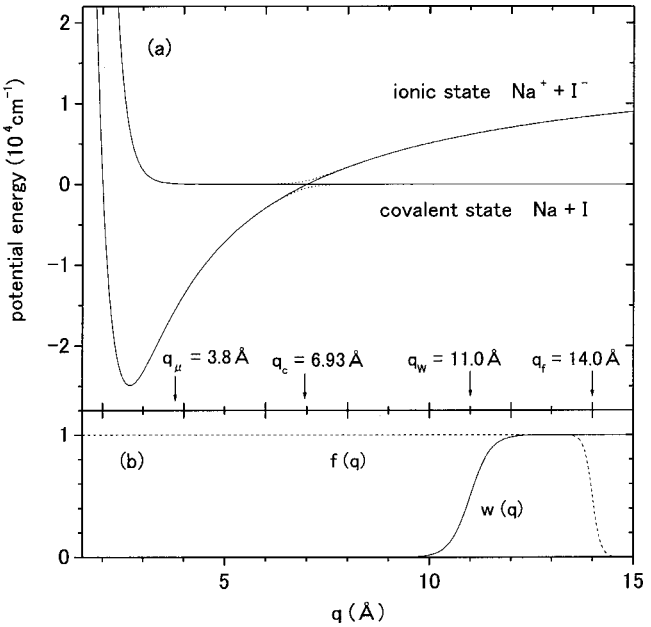

FIG. 1. (a) Diabatic (adiabatic) potential energy curves for NaI (Ref. 17) are drawn by solid (dotted) lines. (b) Functions $f(q)$ [Eq. (36b)] and $w(q)$ [Eq. (37b)] associated with the cutoff function and target operator are also illustrated.

To iteratively solve the coupled pulse design equations, we employ the algorithm developed by Zhu and Rabitz,[5] since it exhibits quadratic and monotonic convergence. As an initial guess field, we assume a Gaussian pulse whose temporal peak is set to $t = 150$ fs, and peak intensity and temporal width are chosen so that about 25% of the population is transferred to the electronic excited state. For the weight parameter, we assume $A = 4.0 \times 10^{11}$. Under these conditions, 100–1400 iteration steps were needed to obtain converged results, depending on the magnitude of the diabatic coupling. In the final two steps, the difference in values of the objective functionals was $\Delta J/J = 10^{-6}\% - 10^{-8}\%$. To save memory as well as computational time, the cutout wave packet data were stored every five time steps. We numerically observed a monotonic convergence behavior of the objective functional as a function of iteration steps (not shown here).

Figure 2 shows (a) a calculated optimal pulse and (b) the population on each diabatic potential as a function of time. As indicated by the dotted line in Fig. 2(b), 95% of the population is transferred into the dissociation continuum. The pulse is composed of three subpulses, each of which controls the molecule in a different way. The first subpulse is a pump pulse that transfers the initial population to the excited electronic state. The second subpulse consists of low-frequency components that strengthen the diabatic coupling to prevent the excited packet from directly dissociating. These two subpulses create an excited packet that has a spatially localized distribution just before it reaches the outer turning point. Note that relevant to this packet shaping, the frequency of the first subpulse is positively chirped, which is in agreement with the results of analysis by Tang and Rice.[30] This shaped packet with an outgoing momentum is then efficiently transferred to the dissociation continuum by the

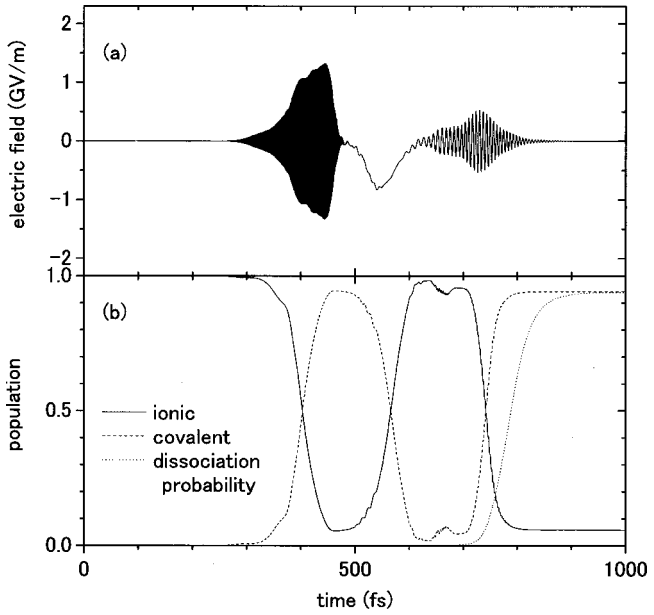

FIG. 2. (a) Calculated optimal pulse and (b) time evolution of the population on each diabatic potential for a preoriented model. The dissociation probability $\langle W(t)\rangle$ as a function of time is presented by a dotted line.

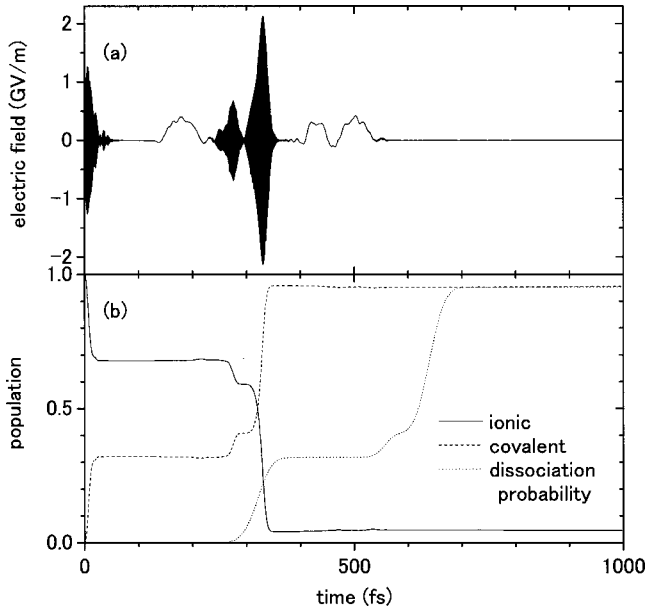

FIG. 3. (a) Calculated optimal pulse and (b) time evolution of the population on each diabatic potential for a preoriented model, when the diabatic coupling is replaced with $V_{ic}(q)/2$.

third subpulse. If the low-frequency components (the second subpulse) are removed, the dissociation probability is reduced from 95% to 85%. In this case, some of the excited population is directly dissociated by the diabatic coupling, which deforms the wave packet remaining on the excited state. This deformation decreases the efficiency of the dumping process and results in a reduction of the dissociation probability. In effect, the sign of the amplitude of the second subpulse is determined so as to strengthen the diabatic coupling in order for the wave packet to time propagate along the excited adiabatic potential.

Finally, we would like to comment on the generation of the low-frequency subpulse shown in Fig. 2(a), which may be called a half-cycle pulse.[30,31] Although half-cycle pulses can be created by several pulse compression techniques relevant to their temporal widths,[31,32] their intensities are usually much weaker than that of the half-cycle pulse shown in Fig. 2(a). It is possible, in principle, to adjust the phases by using phase modulators, but there are no experimental results showing the effectiveness of a technique for controlling the phase of a half-cycle pulse. Although half-cycle pulses with high intensities and definite phases may be experimentally feasible in the near future, they are not available at present. In order for numerical simulations to suit current experimental conditions, Gross *et al.*[14] introduced a filtering procedure into an iterative solution to remove low-frequency components from an optimal pulse. In the present paper, on the other hand, it will be shown that the low-frequency components are naturally eliminated by taking into account rotational effects (a two-orientation model), which will be discussed in Sec. III C.

A. Effects of the magnitude of diabatic coupling on a control pathway

Another interesting control pathway is to utilize the diabatic transitions by weakening the diabatic coupling, contrary to the above-mentioned results. We will show below that the magnitude of the diabatic coupling determines whether the optimal pulse chooses an indirect pathway (pump–dump control) or a direct dissociation pathway. Figure 3 shows (a) a calculated optimal pulse and (b) the population on each diabatic potential as a function of time, when the diabatic coupling $V_{ic}(q)$ is replaced with $V_{ic}(q)/2$. Again, we have a high dissociation probability of 95%. The optimal pulse consists of several subpulses that are either pump pulses or low-frequency pulses. The low-frequency subpulses have opposite signs to that in Fig. 2(a); that is, they negate the diabatic coupling by the optical interaction when the excited packets pass the crossing point. Since these couplings have a different nuclear coordinate dependence, the pulse shape must be adjusted so that the two couplings cancel each other at every nuclear coordinate separation near the potential crossing. This explains the fact that the shapes of the low-frequency subpulses reflect the shapes of the corresponding wave packets. To lower the penalty due to the pulse fluence, all of the subpulses appear separately in time (no temporal overlap).

B. Effects of the reflection of wave packets at the boundary on the control mechanism

In our calculations, the artificial reflection of wave packets at the edge of the grid is removed by the wave function splitting procedure. Here we will discuss the effects of the artificial reflection on optimal pulse shapes and show how they lead to erroneous results without graphical illustrations. In this subsection, we assume the same diabatic-coupling condition as that for the example shown in Fig. 3.

If the system is excited by the pulse shown in Fig. 3(a), but in the presence of a reflecting boundary, a portion of the dissociated packet turns around the boundary, comes back, and goes out of the target (dissociation) region. Thus, in the

presence of a reflecting boundary, the control pathway must be changed to prevent a reduction in dissociation probability due to such a packet reflection. In effect, an optimal pulse calculated under the influence of artificial reflection has a very different structure from that of the pulse shown in Fig. 3(a). This pulse does not choose a direct dissocation pathway, but adopts the pump–dump control pathway. Its shape is quite similar to that of the pulse shown in Fig. 2(a), but the irradiation timing is shifted toward the final time so as to minimize the reflecting components.

A more serious problem arises when the artificially reflected components come back to the optical interaction region, since the optimal pulse can misuse them to enhance the dissociation. As an example, we consider the case in which the final time is set to $t_f = 2000$ fs, which is longer than the period of the excited packet oscillation. The control pulse is composed of several pump, dump, and low-frequency subpulses (not shown here). In the pumping processes, the pulses utilize the interference between the ground-state packet and artificially reflected packets. To numerically check how these fictitious excitation processes reduce the dissociation yield, we calculated the time evolution with an absorbing boundary and found that the probability is reduced to 78%, which is considerably smaller than that of 95% in Fig. 3(b).

C. Orientation effects

So far, we have assumed a preoriented NaI molecule. For a molecule that has the opposite orientation to that discussed so far, low-frequency (half-cycle) pulses can cause opposite effects because of their unipolar nature. That is, a pulse that weakens the diabatic coupling can strengthen it for a molecule that has an opposite orientation.

To discuss orientation effects, we must adopt a three-dimensional (3D) model. If we are concerned with internal dynamics interacting with a linearly polarized electric field, the dynamics is described by the azimuthally symmetric Hamiltonian in the radial–polar space:

$$H^t = -\frac{\hbar^2}{2m}\left[\frac{\partial^2}{\partial q^2} + \frac{1}{q^2}\frac{1}{\sin\theta}\frac{\partial}{\partial\theta}\left(\frac{1}{\sin\theta}\frac{\partial}{\partial\theta}\right)\right] + V(q) - \mu E(t)\cos\theta, \tag{38}$$

where m is a reduced mass, θ is the angle between the NaI axis and the electric field, and $V(q)$ includes all the potentials except the dipole interaction.

In this paper, we present the results of qualitative analysis of the effects of orientation on control. For the purpose of qualitative analysis, the following simplifications are made: (1) the rotational kinetic energy is neglected (a frozen rotational wave packet), and (2) it is assumed that there are two orientation states $|\pm\rangle$ defined by

$$\langle \pm|\cos\theta|\pm\rangle = \pm 1, \quad \langle \pm|\cos\theta|\mp\rangle = 0. \tag{39}$$

Machholm and Henriksen[33] adopted the same two-orientation model in their study on control for selective photofragment orientation of NaI. They found that the numerical results were in good agreement with those obtained by 3D calculations. It is therefore expected that we can qualitatively interpret essential features of the orientational effects based on this simplified simulation.

Within our model, the dynamics is described by the Schrödinger equation

$$i\hbar\frac{\partial}{\partial t}|\Psi(t)\rangle = [H_M + V^t]|\Psi(t)\rangle, \tag{40}$$

where H_M is defined in Eq. (35) and

$$V^t = -\mu E(t)(|+\rangle\langle +| - |-\rangle\langle -|). \tag{41}$$

The projected wave functions defined by $|\psi_\pm(t)\rangle = \langle \pm|\Psi(t)\rangle$ obey

$$i\hbar\frac{\partial}{\partial t}|\psi_\pm(t)\rangle = [H_M \mp \mu E(t)]|\psi_\pm(t)\rangle. \tag{42}$$

If we assume that the molecule is initially in thermal equilibrium and that both orientation states are equally occupied, we have the initial density matrix of

$$\rho(t=0) = |\psi_0\rangle[|+\rangle p_+^{(0)}\langle +| + |-\rangle p_-^{(0)}\langle -|]\langle\psi_0|, \tag{43}$$

where $|\psi_0\rangle$ represents the initial state of the vibronic state of NaI and $p_\pm^{(0)}$ denotes initial thermal distributions with $p_+^{(0)} = p_-^{(0)} = 0.5$. With this notation, the optimal pulse at time t can be expressed as

$$E(t) = -A\,\mathrm{Im}\{p_+^{(0)}\langle\xi_+(t)|\mu|\psi_+(t)\rangle - p_-^{(0)}\langle\xi_-(t)|\mu|\psi_-(t)\rangle\}, \tag{44}$$

where the initial conditions are given by

$$|\psi_\pm(t=0)\rangle = |\psi_0\rangle. \tag{45}$$

The Lagrange multipliers $|\xi_\pm(t)\rangle$ introduced into Eq. (44) represent the constraints due to the equations of motion in Eq. (42) with the final conditions of

$$|\xi_\pm(t_f)\rangle = W|\psi_\pm(t_f)\rangle. \tag{46}$$

Figure 4 shows (a) a calculated optimal pulse and (b) the population on each diabatic potential as a function of time, when the diabatic coupling $V_{ic}(q)$ is replaced with $V_{ic}(q)/2$. We see from Fig. 4(a) that there are no low-frequency components, although they played an essential role for a preoriented molecule (Figs. 2 and 3). The optimal pulse is a pair of pump and dump pulses that transfers 95% of the population to the dissociation continuum. Both subpulses have positively chirped structures (not shown here) to squeeze the excited packet (pump pulse) and to efficiently dump it into the dissociation continuum (dump pulse).

In a previous study by Gross *et al.*,[14] a gradient filtering was introduced to remove low-frequency components from the control pulses. However, such components are naturally eliminated if the orientational effects are taken into account, as shown in Fig. 4. If the control time is sufficiently short to ignore the rotational motion, it is expected that the present two-orientation model accurately approximates the 3D dynamics as mentioned in Ref. 33. We therefore conclude that a pump–dump scheme is the optimal control pathway to enhance the predissociation within one cycle of nuclear vibra-

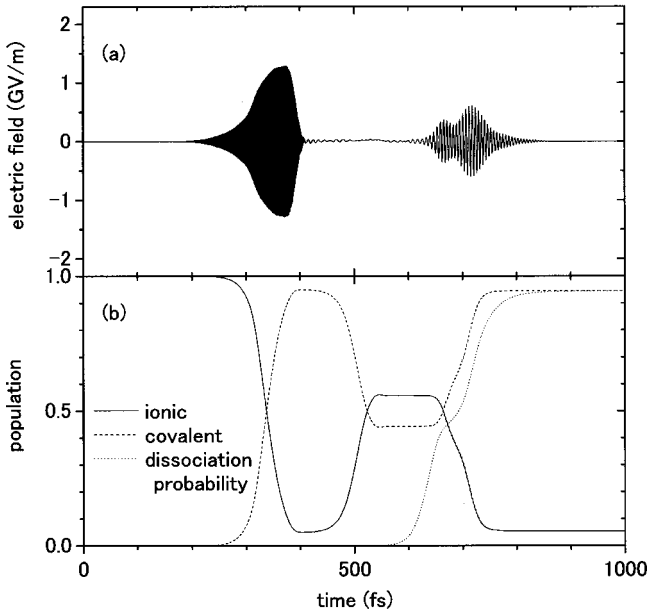

FIG. 4. (a) Calculated optimal pulse and (b) time evolution of the population on each diabatic potential for a two-orientation model, when the diabatic coupling is set to $V_{ic}(q)/2$.

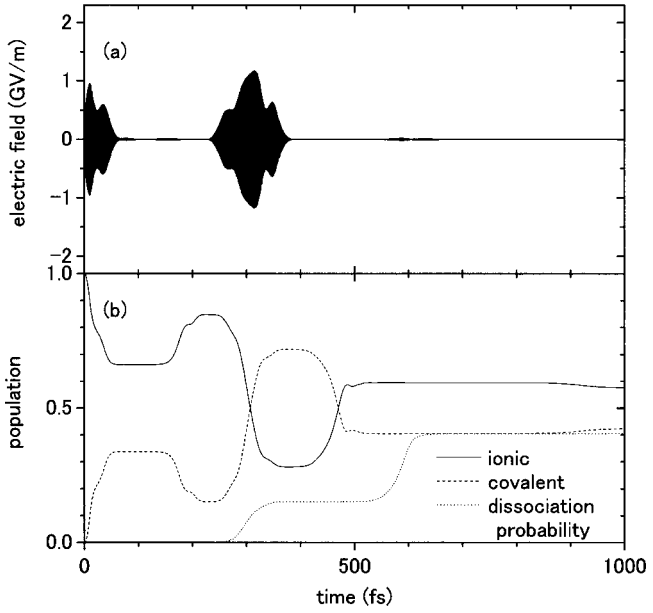

FIG. 5. (a) Calculated optimal pulse and (b) time evolution of the population on each diabatic potential for a two-orientation model, when the diabatic coupling is set to $V_{ic}(q)/2$ and the transition moment function is modified by Eq. (47).

tion. This control mechanism is in good agreement with those discussed on the basis of physical intuitions.[34,35]

Another feature of the optimal pulse is that the delay time between the pump and dump pulses is slightly longer than that of the pulse shown in Fig. 2(a). In Fig. 4, about 45% of the population moves along the covalent potential and directly dissociates, while the wave packet remaining on the ionic potential is transferred to the dissociation continuum by the dump pulse around $t \sim 700$ fs. The directly dissociated packet and dumped packet cannot adjust their phases so as to enhance the optical transitions by constructive interference. Thus the dump pulse has to wait until the directly dissociated packet moves away from the optical transition region for the dumping process. On the other hand, no such restriction is imposed on the timing of the dump pulse in Fig. 2(a) since there is virtually no directly dissociated components. The difference in the delay times, therefore, can be attributed to the difference in the potential coupling strengths.

Finally, we consider the case in which the optical interaction region is restricted so that a control pulse can excite the molecule around the Franck–Condon region accessible from the initial state. That is, the optimal pulse must enhance the predissociation only through pumping processes. For this purpose, the transition moment function is set to

$$\mu(q) = \frac{\mu_0}{1+\exp[\alpha_\mu(q-q_\mu)]}, \tag{47}$$

with $\mu_0 = 3.527$ D, $\alpha_\mu = 16.0$ Å^{-1}, and $q_\mu = 3.8$ Å. In this calculation, the two-orientation model is adopted. The calculated optimal pulse and time evolution of populations are shown in Fig. 5. From Fig. 5(b), we see that the excited packets tend to move along the diabatic covalent potential, and at the final time, 40% of the population is transferred to the dissociation continuum. To examine the control mechanism, we calculated the power spectrum of this optimal pulse, which is shown in Fig. 6. In this calculation, we removed the first subpulse, since the rapid rise in the pulse amplitude around $t \sim 0$ introduces a complicated structure into the power spectrum. For comparison, the power spectrum of the pump pulse in Fig. 4(a) is also shown by a dotted line. The power spectrum is shifted toward a higher frequency than that in Fig. 4(a). That is, the pump pulses in Fig. 5(a) selectively create a wave packet with higher energy in order for the packet to have a larger velocity at the potential crossing and to efficiently cause nonadiabatic transitions (Landau–Zener mechanism). The decrease in the Franck–Condon factor with increase in the excitation frequency imposes a restriction on this control mechanism because it re-

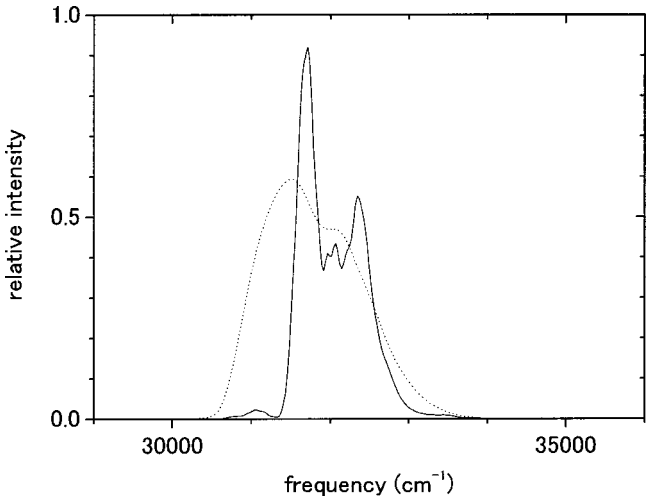

FIG. 6. Power spectrum of the pump pulse in Fig. 4(a) (dotted line) and that in Fig. 5(a) (solid line), in which the spectrum is defined by an absolute square of the Fourier components of an electric field.

quires a more intense pulse that suffers from a larger penalty due to pulse fluence. In addition to the frequency shift, we can see a band structure in the power spectrum (solid line). The spacing between the peaks corresponds to the energy separation of the adjacent bound states in the ground electronic state. This indicates that the pulse may utilize a pump-dump–pump excitation process in order for the packet to acquire larger kinetic energy, which is in agreement with the results reported by Gross *et al.*[14]

IV. SUMMARY

For optimal control of unbounded molecular dynamics, we have developed an algorithm to deal with a spatially delocalized final condition of pulse design equations by combining a target operator having the form of a quasiprojector with a wave packet splitting procedure. Since the quasiprojector can directly specify a spatially delocalized state, optimal pulses are calculated by homogeneous pulse design equations. Our algorithm for treating a spatially delocalized final condition can naturally be combined with the efficient iteration algorithms that were developed for solving the homogeneous type of pulse design equations. Therefore, our algorithm is a powerful tool for dealing with unbounded molecular dynamics such as photodisociation and bimolecular reactions.

The effectiveness of the quasiprojector-type target operator stems from the fact that it does not deform the shape of a wave packet outside the grid region because of the condition given by Eq. (25). According to our algorithm [Eqs. (32)–(34)], backward propagation can be calculated using cutout wave packet data that are stored in memory. Since we can assume a small spatial region, this can considerably reduce the number of grid points and, therefore, computational time. The trade-off is that large memory is needed to store the wave packet data, although the frequency at which wave packet data should be stored and the amount of spatial data that should be stored depend on the numerical accuracy required for each calculation. Looking at recent developments in computer technology, reducing computational time seems to be more important than saving memory in our practical applications.

As an illustrative example, optimal pulses that accelerate predissociation of NaI were calculated under various conditions of potential coupling, transition moment, and orientation. As a prototype of the control of predissociation in polyatomic molecules, in which there exist several competing processes, we aim at accelerating the predissociation—i.e., enhancing the dissociation probability within one cycle of nuclear vibration. For a preoriented model, the calculated pulses include low-frequency components that strengthen or negate the potential coupling depending on the nature of the potential (more adiabatic or more diabatic, respectively). In the former case, the optimal pulse is a pair of pump and dump pulses, while in the latter, the excited packet moves along the diabatic potential and directly dissociates. Within a two-orientation model that may approximate a 3D system, it was shown that the orientation effects eliminated low-frequency components from the optimal pulse and led to a pump–dump pulse as an optimal solution. We therefore concluded that the optimal pathway for our physical objective requires pump and dump pulses, both of which are positively chirped. When the optical interaction region was restricted to around the Franck–Condon region accessible from the initial state, the optimal control pulse utilized the Landau–Zener mechanism to enhance the nonadiabatic transitions, resulting in a high dissociation probability.

In the present paper, although we focused on NaI predissociation, which is a typical example of a half collision, the present algorithm can also be applied to full collision processes.[36]

ACKNOWLEDGMENTS

The authors thank Professor Herschel Rabitz and Dr. Wusheng Zhu for their stimulating discussions. Y.O. acknowledges financial support from Tokuyama Science Foundation. This work was partially supported by Grants-in-Aid for Scientific Research on Priority Areas (A) (No. 12042297) and (A) (No. 14050055) and by a grant for ''Development of high-density optical pulse generation and advanced material control techniques'' from the Science and Technology Agency of Japan.

APPENDIX: PROOF OF EQS. (30) AND (31)

To prove Eq. (30), we divide the time interval $[t_{N-1},t_N]$ into M steps, i.e.,

$$t_{N_j}=t_{N-1}+jdt \quad (j=0,1,...,M;\ t_{N_{j=0}}=t_{N-1},\ t_{N_{j=M}}=t_N), \tag{A1}$$

with $dt=\Delta t/M$. Then the time evolution operator can be expressed as the product of those in smaller time intervals:

$$\begin{aligned} U_N^{(k)}|\Phi_{1-R}^{(k)}(t_{N-1})\rangle &= \prod_{j=1}^{M} \leftarrow U^{(k)}(t_{N_j},t_{N_{j-1}})|\Phi_{1-R}^{(k)}(t_{N-1})\rangle \\ &= \prod_{j=1}^{M} \leftarrow [QU^{(k)}(t_{N_j},t_{N_{j-1}})Q]|\Phi_{1-R}^{(k)}(t_{N-1})\rangle, \end{aligned} \tag{A2}$$

where the arrow indicates time ordering: i.e., operators are ordered from right to left as time increases. Here we have taken into account Eq. (17c) and the precondition [P1] that the packet $|\Phi_{1-R}^{(k)}(t_{N-1})\rangle$ stay in the $1-\mathbf{R}$ region in this time interval. Similarly, we have

$$U_N^{(\ell)\dagger}=\prod_{j=1}^{M} \rightarrow U^{(\ell)\dagger}(t_{N_j},t_{N_{j-1}}). \tag{A3}$$

Utilizing Eqs. (A2) and (A3), we have

$$\begin{aligned} PU_N^{(\ell)\dagger}WU_N^{(k)}|\Phi_{1-R}^{(k)}(t_{N-1})\rangle &= \prod_{i=1}^{M} \rightarrow \prod_{j=1}^{M} \leftarrow PU^{(\ell)\dagger}(t_{N_i},t_{N_{i-1}}) \\ &\quad \times W_B[QU^{(k)}(t_{N_j},t_{N_{j-1}})Q]|\Phi_{1-R}^{(k)}(t_{N-1})\rangle. \end{aligned} \tag{A4}$$

We choose a large number of time steps, M, such that the time evolution operator can be approximated by

$$U(t+dt,t)=\exp\left(-\frac{i}{\hbar}H^t dt\right)$$
$$=\exp\left(-\frac{i}{\hbar}(V+V^t)dt\right)\exp\left(-\frac{i}{\hbar}H_0 dt\right), \tag{A5}$$

where $[t,t+dt]\in[t_{N-1},t_N]$. Here the superscript has been omitted for simplicity. Using the assumption regarding the target operator, Eq. (25), and the preconditions [P1–P3], a part of the product appearing in Eq. (A4) can, for example, be calculated by

$$U^{(\ell)\dagger}(t_{N_M},t_{N_{M-1}})W_B Q U^{(k)}(t_{N_M},t_{N_{M-1}})Q=W_B(dt)Q, \tag{A6}$$

where

$$W_B(dt)=\exp\left(\frac{i}{\hbar}h(x)dt\right)W_B\exp\left(-\frac{i}{\hbar}h(x)dt\right). \tag{A7}$$

Successively applying Eq. (A6) to Eq. (A4), we have

$$PU_N^{(\ell)\dagger}WU_N^{(k)}|\Phi_{1-R}^{(k)}(t_{N-1})\rangle$$
$$=W_B(\Delta t)PQ|\Phi_{1-R}^{(k)}(t_{N-1})\rangle=0. \tag{A8}$$

To prove Eq. (31), we utilize the precondition [P1] that $|\Phi_{1-R}^{(k)}(t_n)\rangle$ stay in the $1-\mathbf{R}$ region after time t_n. Then, by applying the above-mentioned procedure to the left-hand side of Eq. (31), we have

$$PU_{n+1}^{(\ell)\dagger}\cdots U_{N-1}^{(\ell)\dagger}U_N^{(\ell)\dagger}WU_N^{(k)}U_{N-1}^{(k)}\cdots U_{n+1}^{(k)}|\Phi_{1-R}^{(k)}(t_n)\rangle$$
$$=PU_{n+1}^{(\ell)\dagger}\cdots U_{N-1}^{(\ell)\dagger}W_B(\Delta t)QU_{N-1}^{(k)}\cdots U_{n+1}^{(k)}|\Phi_{1-R}^{(k)}(t_n)\rangle\cdots$$
$$=PW_B((N-n)\Delta t)Q|\Phi_{1-R}^{(k)}(t_n)\rangle=0, \tag{A9}$$

which proves Eq. (31).

[1] A. P. Peirece, M. A. Dahleh, and H. Rabitz, Phys. Rev. A **37**, 4950 (1988).
[2] R. Kosloff, S. A. Rice, P. Gaspard, S. Tersigni, and D. J. Tannor, Chem. Phys. **139**, 201 (1989).
[3] S. Shi and H. Rabitz, J. Chem. Phys. **92**, 364 (1990).
[4] W. Zhu, J. Botina, and H. Rabitz, J. Chem. Phys. **108**, 1953 (1998).
[5] W. Zhu and H. Rabitz, J. Chem. Phys. **109**, 385 (1998).
[6] Y. Ohtsuki, W. Zhu, and H. Rabitz, J. Chem. Phys. **110**, 9825 (1999).
[7] Y. Ohtsuki, K. Nakagami, Y. Fujimura, W. Zhu, and H. Rabitz, J. Chem. Phys. **114**, 8867 (2001).
[8] J. Z. H. Zang, Chem. Phys. Lett. **160**, 417 (1989); J. Chem. Phys. **92**, 324 (1990).
[9] R. Kosloff, J. Phys. Chem. **92**, 2087 (1988).
[10] D. Neuhauser and M. Baer, J. Chem. Phys. **90**, 4351 (1989); **92**, 3419 (1990).
[11] T. Seideman and W. H. Miller, J. Chem. Phys. **96**, 4412 (1992).
[12] R. Heather and H. Metiu, J. Chem. Phys. **86**, 5009 (1987).
[13] The cutout wave packet may be time propagated in another routine, e.g., in momentum space (Ref. 12). However, this is not suitable for our present purpose, since we have to transform the wave packet into the coordinate representation to calculate the final condition.
[14] P. Gross, D. Neuhauser, and H. Rabitz, J. Chem. Phys. **96**, 2834 (1992).
[15] J. Somlói, V. A. Kazakov, and D. J. Tannor, Chem. Phys. **172**, 85 (1993).
[16] R. de Vivie-Riedle, K. Sundermann, and M. Motzkus, Faraday Discuss. **113**, 303 (1999).
[17] K. Hoki, Y. Ohtsuki, H. Kono, and Y. Fujimura, J. Phys. Chem. A **103**, 6301 (1999).
[18] K. Hoki, Y. Ohtsuki, H. Kono, Y. Fujimura, and S. Koseki, Bull. Chem. Soc. Jpn. **72**, 2665 (1999).
[19] W. H. Press, S. A. Teukolsky, W. T. Vetterling, and B. P. Flannery, *Numerical Recipes in Fortran* (Cambridge University Press, Cambridge, England, 1992).
[20] S. H. Tersigni, P. Gaspard, and S. A. Rice, J. Chem. Phys. **93**, 1670 (1990).
[21] W. Jakubetz, E. Kades, and J. Manz, J. Phys. Chem. **97**, 12609 (1993).
[22] J. L. Krause, M. Messina, K. R. Wilson, and Y. Yan, J. Phys. Chem. **99**, 13736 (1995).
[23] A. Bartana, R. Kosloff, and D. J. Tannor, J. Chem. Phys. **106**, 1435 (1997).
[24] J. L. Herek, A. Materny, and A. H. Zewail, Chem. Phys. Lett. **231**, 50 (1993).
[25] C. J. Bardeen, J. Che, K. R. Wilson, V. V. Yakovlev, P. Cong, B. Kohler, J. L. Krause, and M. Messina, J. Phys. Chem. A **101**, 9587 (1997).
[26] Y. Ohtsuki, Y. Yahata, H. Kono, and Y. Fujimura, Chem. Phys. Lett. **287**, 627 (1998).
[27] Y. Ohtsuki, H. Kono, and Y. Fujimura, J. Chem. Phys. **109**, 9318 (1998).
[28] V. Engel and H. Metiu, J. Chem. Phys. **90**, 6116 (1989).
[29] We assumed a value of $\mu_0=3{,}527$ D, which is calculated at the equilibrium nuclear coordinate separation using the *ab initio* molecular orbital calculation package GAMESS (Ref. 18); M. W. Schmidt *et al.*, J. Comput. Chem. **14**, 1347 (1993).
[30] H. Tang and S. A. Rice, J. Phys. Chem. A **101**, 9587 (1997).
[31] R. R. Jones, Phys. Rev. Lett. **76**, 3927 (1996).
[32] T. Brabec and F. Krauz, Rev. Mod. Phys. **72**, 545 (2000).
[33] M. Machholm and N. E. Henriksen, J. Chem. Phys. **111**, 3051 (1999).
[34] B. Hartke, E. Kolba, J. Manz, and H. H. R. Schor, Ber. Bunsenges. Phys. Chem. **94**, 1312 (1990); E. Kolba and J. Manz, Faraday Discuss. Chem. Soc. **91**, 369 (1991).
[35] T. Taneichi, T. Kobayashi, Y. Ohtsuki, and Y. Fujimura, Chem. Phys. Lett. **231**, 50 (1994).
[36] A. Abrashkevich, M. Shapiro, and P. Brumer, Chem. Phys. **267**, 81 (2001).